



Pergamon

Acta Materialia 50 (2002) 1627–1638



www.actamat-journals.com

Lattice strain evolution during cyclic loading of stainless steel

T. Lorentzen^{1,a}, M.R. Daymond^{b,*}, B. Clausen^{2,c}, C.N. Tomé^d

^a Materials Research Department, Risø National Laboratory, Roskilde 4000, Denmark

^b ISIS Facility, Rutherford Appleton Laboratory, Chilton, Didcot, Oxon OX11 0QX, UK

^c LANSCE-12, Los Alamos National Laboratory, Los Alamos, NM 87545, USA

^d MST-8, Los Alamos National Laboratory, Los Alamos, NM 87545, USA

Received 4 September 2001; received in revised form 28 December 2001; accepted 28 December 2001

Abstract

A uniaxial tension/compression test specimen was cycled between fixed total strain limits of $\pm 0.4\%$ for eight successive cycles. The sample was loaded using a dedicated Instron hydraulic load frame on the ENGIN station of the PEARL beam line at the ISIS facility of the Rutherford Appleton Laboratory. The load frame was aligned to allow simultaneous monitoring of longitudinal and transverse lattice strain components. There was a strong experimental *hkl*-dependency of the lattice strain response in both the effective stiffness and in the lattice strain loop hysteresis. The experimental data were compared with numerical predictions obtained from a self-consistent elasto-plastic model for the simulation of polycrystal deformation. A cyclic hardening law was developed and implemented into the modelling scheme, providing theoretical predictions in good agreement with experimental observations. © 2002 Acta Materialia Inc. Published by Elsevier Science Ltd. All rights reserved.

Keywords: Bauschinger effect; Neutron diffraction; Elasto-plastic self-consistent model

1. Introduction

The deformation of polycrystalline materials has constituted an important branch of materials science for more than 60 years. Throughout this

period the major focus has been on macroscopic flow curve prediction, texture simulation and yield loci calculation. In recent years the focus has also been directed towards the prediction of the development of lattice strains for differently oriented grains within the polycrystal. This area of interest can largely be attributed to the increased use of neutron diffraction as a tool for studying the micromechanics of polycrystalline aggregates, and for engineering applications such as residual stress characterization [1].

The study of residual stress generation in polycrystals using neutron diffraction has a two-fold aim. First, neutron diffraction is especially

* Corresponding author. Tel.: +44-1235-445434; fax: +44-1235-445720.

E-mail address: mark.daymond@rl.ac.uk (M.R. Daymond).

¹ Currently at DanStir ApS, CAT Science Park, Postboks 30, Roskilde 4000, Denmark.

² Currently at Department of Materials Science, California Institute of Technology, Pasadena, CA 91125, USA.

well matched in the level of detail provided to the validation of current models of polycrystal deformation; that is self-consistent schemes [2] or boundary value solutions [3]. Diffraction, and neutron diffraction in particular, can provide direct experimental evidence of the heterogeneous stress-strain variations evolving in the interior of an elasto-plastic anisotropic crystalline aggregate. Diffraction is therefore an attractive tool to judge, validate and potentially refine the micromechanics on which these modelling schemes rest. The second aim is of a more applied engineering nature, where an increased knowledge of the non-linear and highly anisotropic development of lattice strains and residual intergranular strains can provide essential guidance for engineering studies of residual stresses.

This combined theoretical and experimental approach has already been successfully used in the study of in situ uniaxial deformation. Current state-of-the-art modelling has been demonstrated recently [4] and correlated with neutron diffraction experiments on steel in a subsequent publication [5]. Holden et al. [6] have illustrated the role of polycrystal modelling in the interpretation of measured residual strains in Ni-based alloys. In these systems the strong directional dependence of elastic and plastic response, combined with the crystallographic texture, makes it very difficult to deconvolute residual strains using only the raw information of lattice strains. We have also demonstrated the potential of the anisotropy in lattice strain response of different *hkl* directions to hold a “fingerprint” of the deformation history [7].

Previously reported work [5,7] has demonstrated that the *hkl*-dependency of the residual intergranular stresses is of utmost importance in the proper analysis of diffraction-based measurements of residual stress in engineering components. However, these previous studies were limited to unidirectional, uniaxial loading situations, whereas engineering structures typically undergo cyclic and multiaxial loading. As the findings from these initial studies cannot be directly applied to the more general cyclic and/or multiaxial case, it is necessary to extend these kinds of studies, and a natural first extension is cyclic uniaxial loading.

The highly anisotropic generation of residual

intergranular stresses plays an important role in the Bauschinger effect; the present experiment enables us to correlate these quantities in a direct manner. The Bauschinger effect is of both scientific and engineering interest, and constitutes an effect of relevance to many industrial processes where material undergoes forward and reverse loading. For instance, in sheet metal forming it is well known that some stages of the deformation which the material undergoes include successive bending and straightening. As in true composites, where the inhomogeneity of phase-specific internal stresses plays a dominant role in the evolution of the Bauschinger effect, in pure metals the dependence of residual intergranular stresses on crystallite orientation and anisotropy affects the material's Bauschinger effect. In correlating these residual intergranular stresses with the macroscopic evolution of the Bauschinger effect, it is envisaged that by careful tailoring of, for example, the material's texture, coupled with control of the magnitude of residual intergranular stresses, specific Bauschinger effects may be tailored for specific engineering purposes such as compensating for spring-back effects.

Apart from this relevance to engineering purposes, the experiments provide a direct evaluation of models of polycrystal deformation. This desire to pursue a more materials science-based aspect is in fact driven by the ultimate goal of establishing better constitutive models of materials' behaviour. In contrast to the phenomenological approach of continuum mechanics, it is a central goal for materials scientists to define material models based on actual micromechanical and physical phenomena which are observed in the microstructures of the material. The scale at which we consider the characteristics of materials deformation originates at crystallographic slip in the atomic lattice and is subsequently, through the evolution of lattice strains and stresses, extended to the overall macroscopic elastic and plastic behaviour of the aggregate, including the prediction of material yield surfaces. Recent work [8] deals with polycrystal simulations of cyclic loading using a Lin–Taylor upper-bound approach, and concentrates mainly on the macroscopic response of the aggregate. To the authors knowledge, however, the present work rep-

resents the first attempt at measuring and simulating the evolution of lattice strain during cycling, although reverse yielding in MMCs has been studied by Pragnell et al. [9].

2. Experimental details

The material used in the present investigation is an fcc stainless steel cut from the same sheet to the one used in [5], where further details on the chemical composition, strength and stiffness data can be found. The sample geometry was a specimen of diameter 7 mm and gauge length 25 mm designed as a compromise between the necessity of a limited aspect ratio to allow the compression part of the cycles, and sufficient space between the mounting grips to allow unhindered passage of the incident and diffracted neutron beams. Incident slits 5×5 mm were used, with the outgoing beam defined using radial collimation of width 1.5 mm. Since only the central part of the specimen is thus measured by the neutron beam, the diffraction results should be insensitive to any inhomogeneity of deformation sometimes found in reverse-loading tests [9].

The experimental configuration used a purpose-built Instron loading frame mounted on the diffractometer [10], with its loading axis 45° to the incident beam, allowing the simultaneous monitoring of both longitudinal and transverse diffraction patterns using two detector banks. A schematic illustration of the arrangement is given in Fig. 1.

The sample was mounted with a standard clip-gauge extensometer to monitor the macroscopic strain in the loading direction during the neutron tests. The experiment was conducted as an incremental loading under load control, cycling the materials between fixed strain limits of approximately ±0.4%. Diffraction data were then collected at each increment in load.

During the initial three cycles diffraction patterns were monitored at approximately 24 load levels during each cycle. Thereafter, diffraction patterns were collected only at the extreme tensile and compression levels, and when passing through zero load. To collect the diffraction patterns (from the left- and right-hand detector banks) took approxi-

mately 40 minutes, in order to acquire sufficient statistical quality to allow accurate d-spacing determination for at least six independent *hkl*-reflections. In total, the whole experiment progressed over more than 72 hours. A typical diffraction pattern is shown in Fig. 2.

3. Experimental results

The experimental lattice strain loops for six independent *hkl*-reflections were measured, and some of these are shown in Figs. 3 and 4, covering the longitudinal and transverse strain components, respectively. All data shown are based on single peak fitting using a standard non-linear least square fitting procedure. The peak fitting incorporated the wavelength-dependent anisotropic peak shape found at pulsed neutron sources [11], using the GSAS software [12].

Fig. 3a–c illustrate a number of clear points. The small but non-zero intergranular strains, i.e. near-linear strain for macro applied stress, which has been observed for the 111 and 311 diffraction peaks in uniaxial tests [5,7], is seen here throughout the tensile–compressive cycling, and this was also true for the 420 peak. These same peaks also demonstrate a linear behaviour in the transverse direction (Fig. 4a,b). On the other hand, in the axial direction a clear hysteresis is observed in the 200 and 331 peaks in particular, and also to a lesser extent in the 220. These responses are in qualitative agreement with the relative magnitude of plasticity-induced intergranular strains observed in unidirectional tests carried out earlier [5]. As might be expected, since they are primarily caused by Poisson constraint effects, the magnitude of hysteresis strains is smaller in the transverse direction, though clearly present in the 200 plane. In the 331, 220 and 420 planes in the transverse direction (not shown), any hysteresis is too small to be visible above the experimental scatter of the data.

Although the initial loading event shows a different stress–strain response to the following cycles (particularly clear in the case of axial 200), the loop histories all appear to lie on top of each other, at least within the uncertainty of the measurements. That is, the intergranular response

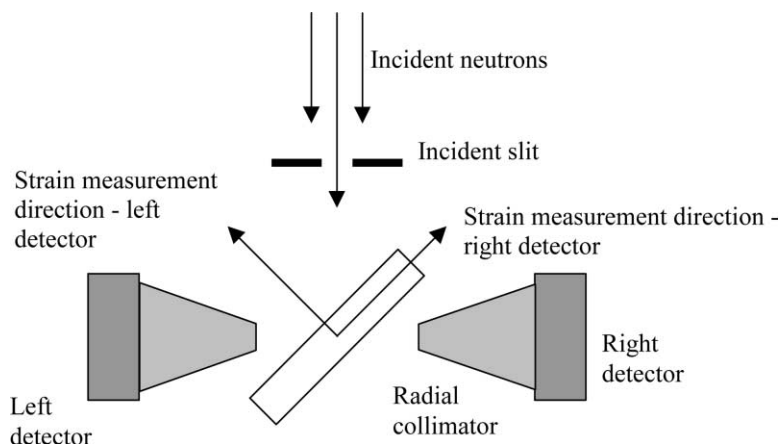


Fig. 1. Experimental configuration of the ENGIN instrument on the PEARL beam line at ISIS. The long axis of the sample is the loading direction. The strain measurement directions for each detector indicate how strains are measured parallel (*right*) and perpendicular (*left*) to the loading axis.

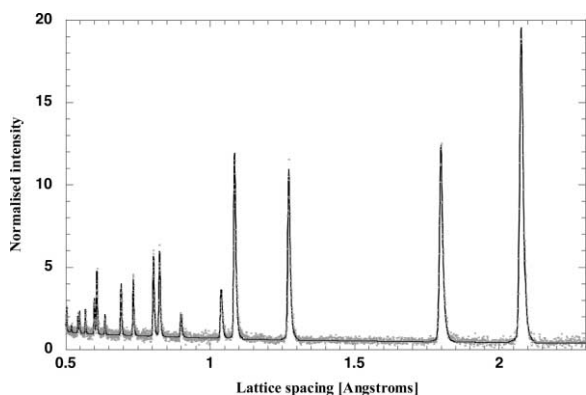


Fig. 2. Typical diffraction pattern collected during the tests. This spectra is taken from the first zero load level, i.e. the as-received sample. Experimental data are shown as grey crosses, the black line is a Rietveld refinement fit to the data.

appears to saturate after a single loop. This can be seen in the close-up of the 200 plane response shown in Fig. 3d. This figure shows the initial loading curve, the first loop and the start of the second, just in the tensile quadrant. Thicker arrows indicate later stages of loading. The first loop clearly follows a different path to the initial loading, but the second loop is almost coincident with the first and, by the plastic strain regime, within experimental uncertainty indeed it is. This is perhaps surprising since the macroscopic stress–strain curve certainly does develop measurably between

the first and last cycles, and we will return to this point.

The macroscopic response shows an identical gradient during cycling on either side of zero applied stress, with macro plasticity occurring only once a significant (~ 100 MPa) reverse stress has been applied. The same unchanging gradient is seen for some of the reflections in the axial direction, namely the 111 and 420, and possibly the 220. On the other hand, there appears to be a distinct change in gradient as the applied load passes through zero for the 200 and 331, and possibly 311, directions. Unfortunately, the data are somewhat sparse for loads immediately following zero, but it is apparent that the response changes at relatively small applied reverse loads.

4. Self-consistent modelling

A self-consistent polycrystal deformation model [13] has been used to predict the measured lattice strains. The model includes the single crystal elastic anisotropy of the stainless steel, and describes the plastic deformation as being caused solely by crystallographic slip on the $\langle 111 \rangle$ –(110) slip planes of the *fcc* lattice. The change of hardening as a function of accumulated strain is described using a kinematic hardening law based on a Voce-type hardening. As the hardening coefficient on a

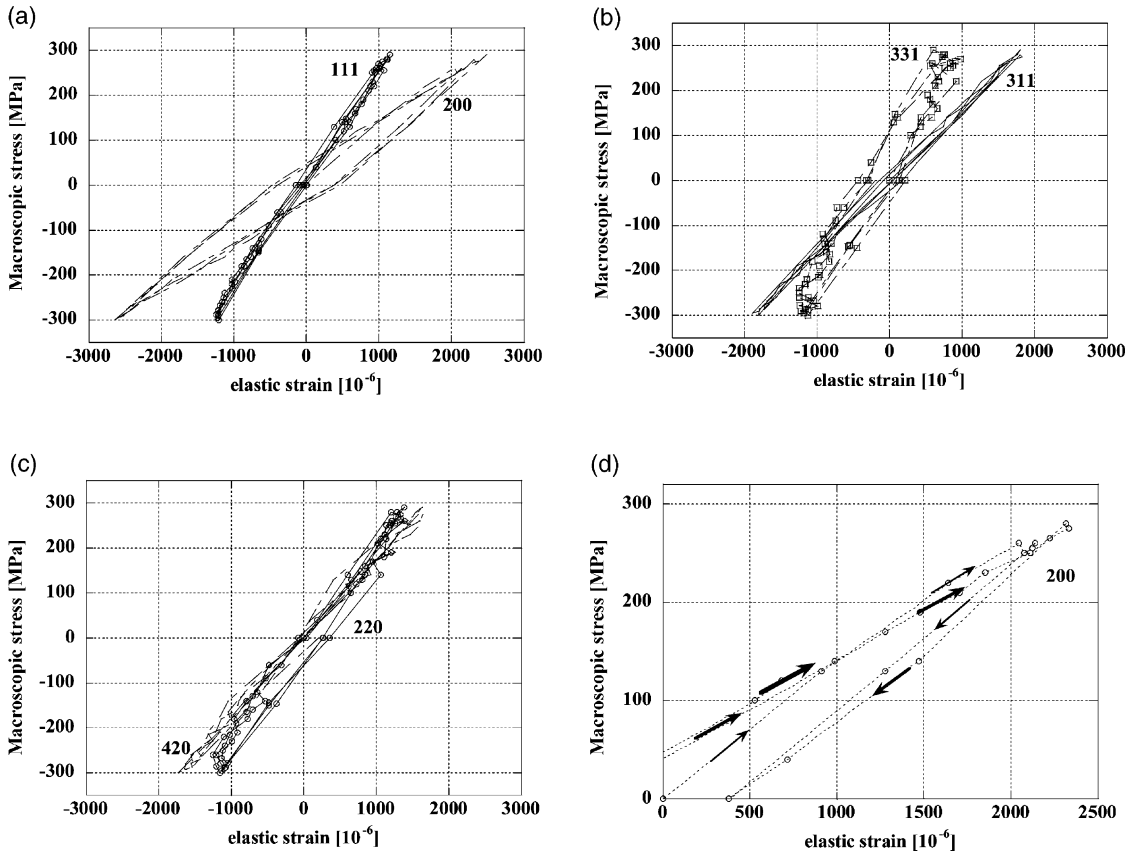


Fig. 3. Experimental data representing the longitudinal lattice strain loops for four six *hkl*-reflections (uncertainties in italics): (a) (200)— $80\mu\epsilon$ and (111)— $70\mu\epsilon$, (b) (311)— $80\mu\epsilon$ and (331)— $175\mu\epsilon$, (c) (220)— $130\mu\epsilon$ and (420)— $175\mu\epsilon$ and (d) close-up of the tensile part of the (200) response at the start of the experiment. Thicker arrows indicate later cycles.

slip system that is loading is increased, the hardening coefficient on the opposite slip system, i.e. the same slip plane but opposite slip direction, is decreased by the same amount. This is a polycrystal plasticity equivalent to the classical macroscopic kinematic hardening law. The main difference with macroscopic kinematic hardening is that this describes a shift of the entire yield surface. In our case, however, we move only the opposite slip direction—the yield surface in other slip directions is unaffected. However, we believe that this is more representative of the “true” material, since it correlates with the reversal of dislocations on a given slip plane.

The hardening function used for each system is thus described by Eq. (1):

$$\hat{\tau}^s = \tau_0^s + (\tau_1^s + \theta_1^s \Gamma) \left[1 - \exp\left(-\frac{\theta_0^s \Gamma}{\tau_1^s}\right) \right] \quad (1)$$

where Γ is the accumulated shear strain in the grain. The threshold stress τ^s in Eq. (1) describes (in an average way) the resistance to activation that the deformation modes experience; it usually increases with deformation due to strain-hardening. Equation (1) represents an extended Voce law which, instead of stress saturation, exhibits an asymptotic hardening rate θ_1^s . For the strains used in this work it is an adjustable hardening parameter. In addition, we allow for “self” and “latent” hardening by defining coupling coefficients $h^{ss'}$ which account for the obstacles that dislocations in system s' represent to the propagation of s dislo-

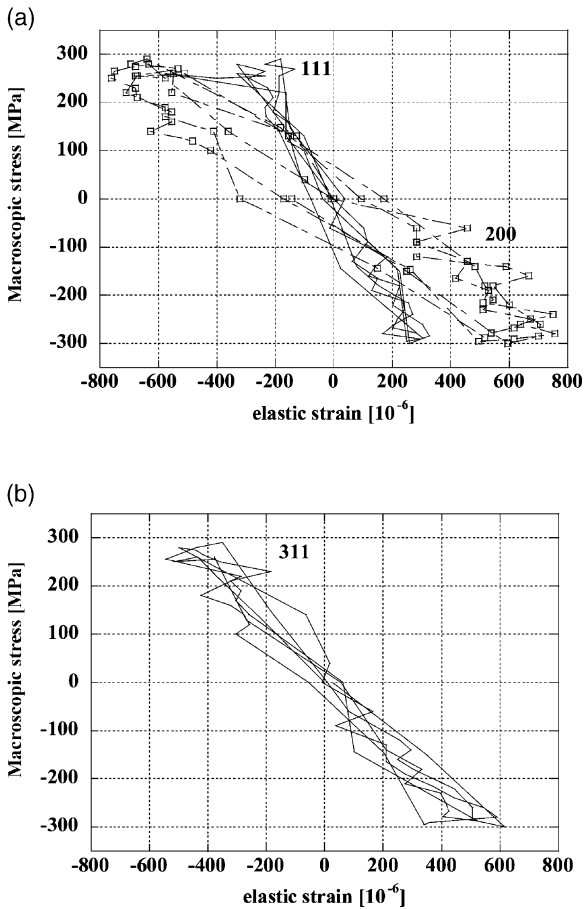


Fig. 4. Experimental data representing the transverse lattice strain loops for three *hkl*-reflections (uncertainties in microstrain in italics): (a) (200)— $110\mu\epsilon$ and (111)— $90\mu\epsilon$ and (b) (311)— $100\mu\epsilon$.

cations. The increase in the threshold stress of a system due to shear activity in the grain systems is calculated as:

$$\Delta\tau^s = \frac{d\hat{\tau}^s}{d\Gamma} \sum_{s'} h^{ss'} \Delta\gamma^{s'}. \quad (2)$$

When “self” and “latent” hardening are indistinguishable, $h^{ss'} = 1$. Equations (1) and (2) permit a description of the high hardening rate observed at the onset of plasticity, and its decrease towards saturation at large strains. Linear hardening is a limiting case of this law, and takes place when $\tau_1^s = 0$.

We add the additional constraint that if a system is loading, i.e. $\tau^s \geq \mu^s \sigma$ and $\dot{\tau}^s \geq \mu^s \dot{\sigma}$ (where μ^s is the Schmidt tensor for slip system s), the hardening on the system with opposite slip direction, s' , is decreased by the same amount:

$$\dot{\tau}^{s'} = -\dot{\tau}^s. \quad (3)$$

By using this definition, only the slip systems opposite to loading systems are experiencing softening, somewhat mimicking the easy reversal of dislocation pile-up on loading slip systems. All the other systems harden the same as the forward slip system. As a consequence, except for the special treatment of the opposing system, this is an isotropic model (i.e. $h^{ss'} = h^{ss}$) without latent hardening. We acknowledge that a permanent displacement of the opposite facet in the single crystal yield surface is a simplistic way of dealing with the reversible back-stresses associated with pile-ups. We expect, however, to be able to reproduce the Bauschinger effect through this mechanism.

The elastic properties of the steel are based on published data, as described in [5]. The choice of optimal parameters for the critical resolved shear stress and hardening coefficients is made in an iterative approach aimed at achieving the best possible agreement with the observed macroscopic cyclic behaviour. The philosophy is that we do not proceed to study microstructure-related features until the model has proven a capacity to reproduce the observed macroscopic behaviour of the aggregate (Fig. 5a). Some development in the experimental macroscopic loop can be observed and for the optimization of the model predictions compromises had to be made when defining the parameters of the hardening law. The level of hysteresis reduces as cycling occurs, as the system becomes plastically stiffer, but also as plasticity occurs at slightly lower stresses. As can be seen in Fig. 5b, the model macroscopic loop also clearly develops under cycling; the model has been optimized to predict macroscopic loops closely resembling the experimental observations. It correctly captures the major features of the change in shape of the hysteresis loop, namely earlier initial hardening and stiffer plastic strain gradient. However, although not shown in the figure, the experimental macroscopic loop appeared to stabilize, or at least the

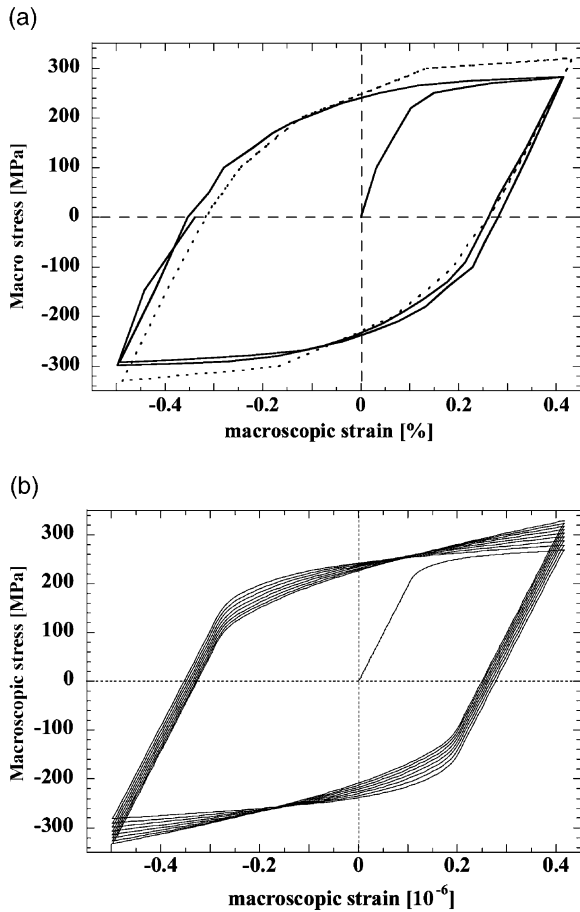


Fig. 5. (a) The development in the macroscopic stress–strain loop, showing the first two cycles (*continuous line*) and the eighth cycle (*broken line*) and (b) the subsequently predicted macroscopic loop closely resembling these observations.

change in shape from cycle to cycle was reduced with each cycle; thus cycle 7 and cycle 8 were identical within the uncertainty in measurement. In contrast, it is apparent that the model hysteresis loop continues to change in shape, and while there is a slight reduction in the rate of change as cycling progresses, this effect is relatively small. The reasons seems to be that, because of grain interaction effects, the macroscopic stress reversal is not necessarily accompanied by a microscopic stress reversal in the grains. As a consequence, it is not necessarily the opposite system that is activated in reversal, and the mechanism of dislocation recombination is not mimicked in all grains.

Based on achieving agreement with the macroscopic behaviour as far as possible, we proceed to extract from the simulation data corresponding to the volume-weighted averages of the elastic lattice strains in families of “grains” representing the *hkl*-reflections considered in the experimental data, and directly comparable to the grain families sampled in a diffraction experiment. These volume averages form the basis of our predictions of the lattice strain loops, which may be compared to the experimental results of Figs. 3 and 4.

The models show a gradual development of plastic hysteresis behaviour as a function of accumulated plastic strain in the system, both at the macroscopic and intergranular level, while as expected in a model without damage, no change occurs to elastic stiffness.

5. Comparison between model and experiment results

In a qualitative sense the model and experimental results are in good agreement. The planar elastic stiffnesses are of course well predicted. The relative magnitudes of intergranular strains are also correctly determined, with the continued linear behaviour of the 111 and 311 in both axial and transverse directions during cycling correctly captured. The values of the total elastic strains obtained at the maximum applied macroscopic strains are also in good agreement for each lattice reflection.

However, a number of distinct differences can be seen between the model and experimental results. While the macroscopic stiffness and total strains are well captured, the hardening development is not fully described by the model, which can be clearly seen in the gradual change of shape of the modelled macroscopic hysteresis curve. There are also differences between model predictions and experimental measurements of the internal intergranular strains. First, the model shows a distinct development of the magnitude of lattice strain at a particular applied stress with progressive loops; this change is larger than the experimental uncertainty. This effect is particularly clear in the case of the axial 200 peak, where the

maximum change between the first and the eighth cycles corresponds to around three or four hundred microstrain.

Second, there are subtleties in the changes of internal strain gradients at various stages of the cycling. Experimentally, in unidirectional tests [7] and in the initial tensile loading stage of this test, the axial 200 exhibits a clear three-stage behaviour—elastic loading, gradual development of plasticity, and plastic loading. This behaviour is correctly captured by the model; however, the same response is still in evidence in the model predictions during continued cycling. On initial inspection the experimental 200 loops do not show this behaviour, instead exhibiting only two clear gradients—the elastic, and then one corresponding to the second plastic gradient. However, given the lack of experimental data in the region just past zero applied stress, it is more likely that this “kink” is in fact occurring at very low applied stresses. The curvature of the 111 and 311 peaks is correctly captured as being small in both model and experiment. The magnitude of the 220 loop is reasonably captured, while the behaviour of the 331 is over-emphasized by the model; the changes in gradient are much less pronounced experimentally. The one reflection which the model qualitatively fails to capture is the 420, which experimentally exhibits negligible hysteresis compared to the quite significant levels predicted (Fig. 6).

The difference in applied stresses at which inflections in the internal strain occur accounts for the difference in the magnitude (width) of the hysteresis loops for the 200 in model and experiment. The model also overestimates the size of the hysteresis loops in the 220 and 331 planes. The experimental internal strains appear to stabilize after a small number of cycles, whereas the model data predict continued development of the *hkl* strain loops. There is a gradual reduction in the rate of change of the model loops but, in common with the macroscopic hysteresis loops, this change is prolonged over many more cycles than is observed experimentally (Fig. 7).

We should note, however, that the complete loop data are only available for the first three experimental cycles. However, we do have the maximum, minimum and zero stress *hkl* strains for

further cycles; a plot of the 200 residual strains measured at zero applied stress and compared with model predictions is shown in Fig. 8a. The experimental strains do appear to show a small development, barely larger than experimental uncertainty, while on the other hand the model does not show any change in strains observed at zero load with continued cycling. Instead, changes in the model hysteresis loop are seen at elevated stresses (150–250 MPa). It is also worth noting that these experimental results demonstrate an increase in the area of the hysteresis loop, as both tensile and compressive residual strains increase in magnitude, whereas the model data in fact show a decrease in the size of the loop as initial yield occurs at a (slightly) earlier applied stress. Comparison of experimental data in the transverse direction with the corresponding model predictions results in broadly the same conclusions as have been drawn above, although the relative uncertainty in strains in this direction is larger. It is notable, however, that the model transverse loops do show some quite considerable increase in hysteresis area for all but the 311 direction. This is an interesting point, as loops exhibiting hysteresis must involve energy dissipation. An understanding of the relationship between grain orientation and energy dissipation will be crucial in understanding the effect of polycrystalline anisotropy on fatigue behaviour.

We can conclude from this comparison between experimental and theoretical data that while the model broadly captures the behaviour of the polycrystal under cyclic loads, a number of important features are not in full agreement. The fact that agreement is good in the elastic regimes and at the largest plastic strains is important. In earlier unidirectional loading tests [5,7], it was shown that the initial hardening behaviour of the material, which was dependent on initial redistribution of load between different grain orientations, was important to explain the initial changes in slope of intergranular strains. However, at larger plastic strains (>0.2%) the intergranular strains were once again approximately linear with applied stress, though with a different gradient to the elastic regime. Hence we can imply that it is during the redistribution of strains between different lattice directions at small plastic strains that the model is

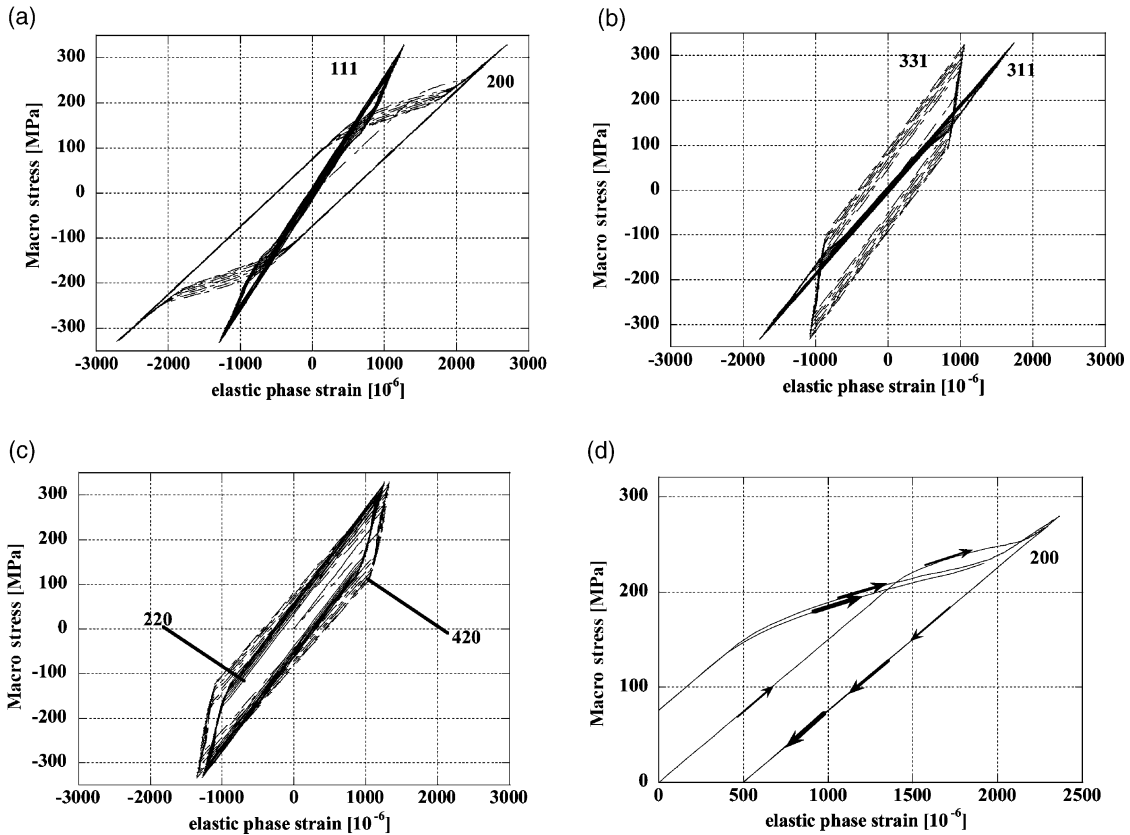


Fig. 6. Simulated longitudinal lattice strain loops for four hkl -reflections: (a) (200) and (111), (b) (311) and (331), (c) (220) and (420) and (d) close-up of the tensile part of the (200) response at the start of the experiment. Thicker arrows indicate later cycles.

failing. This is undoubtedly due to problems with the hardening model. Perhaps one cause of this is that we have not decoupled the back-stress increment (Eq. (3)) from the shear strain increment, but have maintained a strict kinematic description. Another is likely to be the use of isotropic hardening; that is, apart from the opposite slip direction, slip along a particular slip direction causes equal hardening of all the other slip systems in the grain.

6. Plastic anisotropy strain

The data presented above are based on single peak fitting, but using the standard Rietveld refinement technique [14], we can in fact simultaneously fit to the entire diffraction pattern. There-

fore, this approach can be used to provide further information regarding the inherent anisotropy and hkl -dependency on the lattice strain development. In the normal Rietveld refinement of diffraction data the measured intensity distribution as a function of lattice parameter is assumed to be that based on an ideal known crystal structure, such as fcc , bcc or hcp , and the best fit to match this structure is readily calculated. However, as a consequence of deformation, whether it be thermal, elastic or plastic, the physical relationship between the position of different hkl -diffraction peaks deviates from that which would be expected using this ideal structure. During uniaxial elastic deformation, diffraction lines move according to their specific stiffness, which may be described by the so-called A_{hkl} parameter, or by the Kröner stiffness [15]. This does not strictly represent a distortion of a given

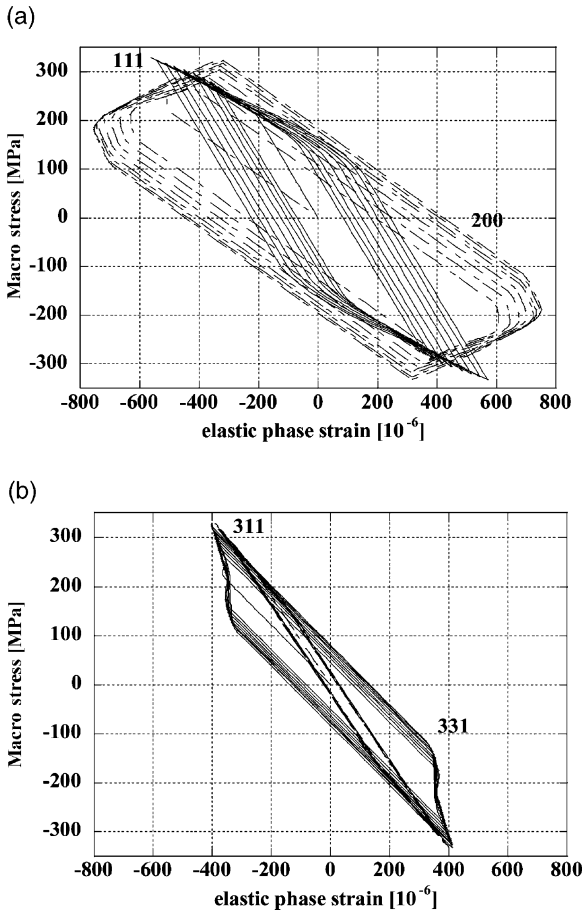


Fig. 7. Simulated transverse lattice strain loops for four hkl -reflections: (a) (200) and (111), (b) (311) and (331).

atomic lattice, just the fact that the mean stiffness of the population of grains in the polycrystal contributing to a particular diffraction peak is, for most materials, dependent upon their orientation. This effect has been introduced into the Rietveld refinement by incorporating so-called *anisotropy strain*, through a new fitting parameter, γ in the refinement [7]. The quantity by which specific diffraction lines shift according to their elastic stiffness is hence governed by the term γA_{hkl} . Rather than refining the diffraction pattern towards an ideal undistorted crystal structure, it is now modified so that, in a particular specimen direction, the lattice parameter tracks the $\langle h00 \rangle$ -direction and other reflections are assumed to deviate from this ϵ_{h00} -term according to Eq. (4):

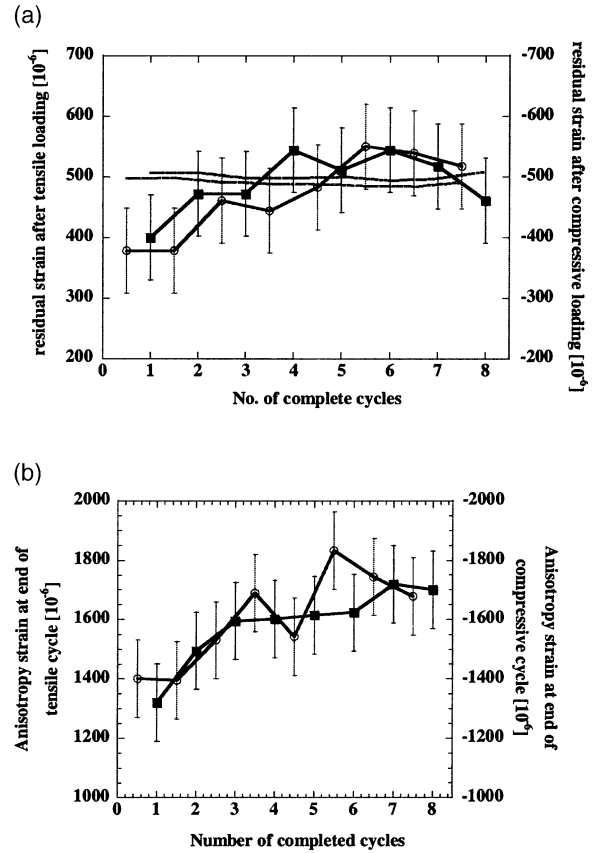


Fig. 8. The residuals measured at zero applied stress for (a) the (200)-reflection and (b) the anisotropy strain. The left-hand scale shows the strain after a tensile cycle (*open symbols*), the right-hand scale strain after a compressive cycle, with reversed axes (*closed symbols*). The (200)-reflection data also show the model predictions, as the lines without error bars, where the lower line corresponds to the tensile data.

$$\epsilon_{hkl} = \epsilon_{h00} - \gamma A_{hkl}. \quad (4)$$

In a quasi-isotropic polycrystalline material, in either a Reuss [16] or Kröner [15] approximation, the general form of Eq. (4) holds [17], based on the fact that the inverse of the polycrystalline plane-specific modulus E_{hkl} is linear with A_{hkl} . The actual values of the linearity constants depend on the grain interaction model used and do not concern us since they are simply treated as fitting parameters.

In the elastic regime this anisotropy strain component (γ) should thus develop linearly and correlate solely with the elastic anisotropy factor A_{hkl} of the material. As soon as the polycrystal

deformation exceeds a limit where elastic anisotropy according to A_{hkl} can no longer explain all deviations from the ideal crystal structure, the fitted anisotropy strain is expected to start deviating from this linear behaviour. This has been shown by Daymond et al. on a data set taken during in situ uniaxial loading of a stainless steel sample [7]. The expected deviation from the initial linear behaviour was observed to correlate directly with the commencement of any noticeable deviation from linearity in the hkl -specific lattice strain response, and also with deviation from linearity (elasticity) in the macroscopic response. It was moreover suggested that the fitting parameter γ could be split into an elastic and a plastic component, $\gamma = \gamma_{ei} + \gamma_{pi}$.

This definition of an anisotropy strain has been used in analysis of the present data set obtained during cyclic deformation, and the calculated anisotropy strain loop shows interesting features as seen from Fig. 9a. First, as with the macroscopic loading curve there is a different loading path for the initial loading event compared with the subsequent cycles. Second, there is a strong hysteresis in the cyclic loading, and even in the space of the first three cycles the change in this hysteresis is observable. Furthermore, the change in slope of the anisotropy strain corresponds to just before the start of macroscopic plastic straining, as was indicated by the changes in gradient of the single peak responses. This effect can be particularly clearly seen in Fig. 9b, where the macroscopic plastic strain is compared with γ_{pi} as a function of the applied stress. The plastic anisotropy strain is linear with applied stress in the plastic regime, although the macroscopic plastic strain shows a change in gradient. Thus the approximately linear correlation between γ_{pi} and macroscopic plastic strain observed in [7] for uniaxial linear loading is not completely duplicated in the case of cyclic loading. It should also be noted that the plastic anisotropy loop expands (i.e. shows greater hysteresis) upon continued cycling.

The development of anisotropy with continued cycling can also be seen when only zero-stress data are shown, Fig. 8b. Since these data of course just come from an analysis of the diffraction data, it suggests that indeed a gradual increase in the strain

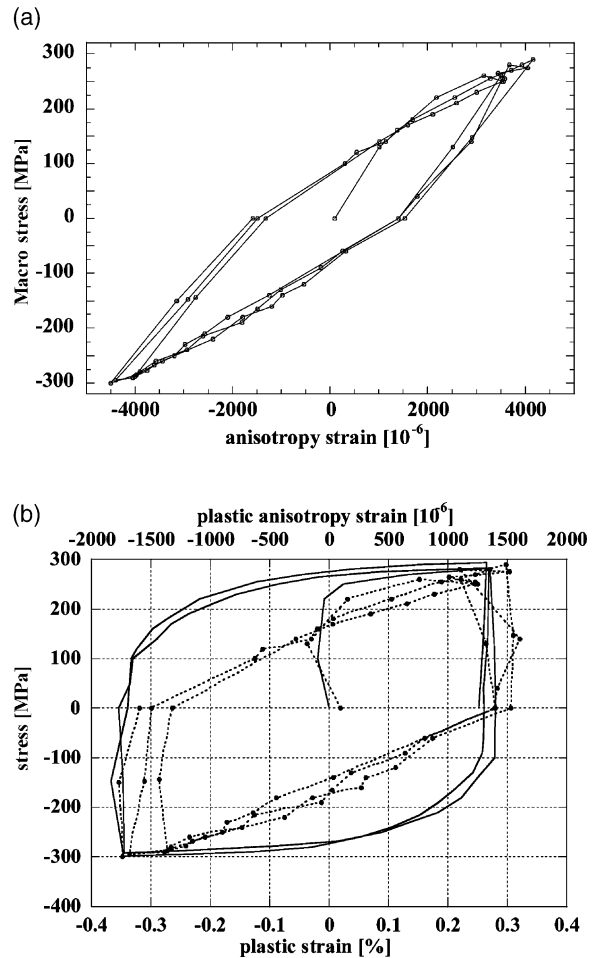


Fig. 9. (a) The anisotropy strain loop obtained from analysis of the experimental data. (b) Comparison of plastic components of anisotropy strain (broken line) and macroscopic strain (continuous line).

hysteresis of, for example, the axial 200 peak must be occurring. The difference here is that by analysing the entire diffraction pattern of many peaks with only two fitting parameters, one can obtain smaller uncertainties, highlighting the small strain changes observed. Due to the still significant uncertainty, however, it is not possible to be certain if any saturation is occurring—this will require the completion of many more cycles.

7. Conclusions

A uniaxial tension/compression test specimen was cycled between fixed total strain limits of $\pm 0.4\%$ in situ on the ENGIN diffractometer at ISIS. Experimentally determined longitudinal and transverse strain components have been compared with numerical predictions obtained from a self-consistent modelling scheme, including a representation of kinematic hardening at a crystal plasticity level. A strong *hkl*-dependency of the lattice strain response in both the effective stiffness and in the lattice strain loop hysteresis was observed in both experimental and theoretical data. Good overall agreement was achieved between model and experimental data. However, several discrepancies were highlighted, which were attributed to deficiencies with the mechanism of modelling the hardening behaviour. Introducing a permanent (negative) hardening rate in the opposite to the active system permanently modifies the single crystal yield surface, and can only be reversed if the opposite system is activated upon macroscopic load reversal. We know, however, that intergranular stresses prevent many grains from unloading through the origin. As a consequence, the opposite system is not necessarily activated during reversal, and the change in the single crystal yield surface becomes permanent rather than reversible. Improving the model will require accounting for intragranular microstructural features in a more realistic

way. We envisage incorporating the effect of back-stress upon the active dislocation source in a manner that will increase the resolved shear upon loading and will reverse such an effect as soon as unloading of the system starts to take place.

References

- [1] Hutchings MT. *Nondestruct Test Eval* 1990;5:395–413.
- [2] Hutchinson JW. *Proc R Soc London A* 1970;319:247–72.
- [3] Asaro RJ, Needleman A. *Acta Metall* 1985;33(6):923–53.
- [4] Clausen B, Lorentzen T, Leffers T. *Acta Mater* 1998;46(9):3087–98.
- [5] Clausen B, Lorentzen T, Bourke MAM, Daymond MR. *Mater Sci Eng* 1999;259(1):17–24.
- [6] Holden TM, Holt RA, Tomé CN. *Mater Sci Eng A* 2000;A282:131–6.
- [7] Daymond MR, Bourke MAM, Von Dreele RB, Clausen B, Lorentzen T. *J Appl Phys* 1997;82(4):1554–62.
- [8] Toth LS, Molinari A, Zouhal N. *Mech Mater* 2000;32:99–113.
- [9] Prangnell PB, Downes T, Withers PJ, Lorentzen T. *Mater Sci Eng* 1995;A197:215–21.
- [10] Daymond MR, Priesmeyer HG. *Acta Mater* 2002;50:1613–1626.
- [11] Von Dreele RB, Jorgensen JD, Windsor CG. *J Appl Crystallogr* 1982;15:581–9.
- [12] Larson AC, Von Dreele RB. *GSAS—General Structure Analysis System*. Los Alamos National Laboratory, 1994.
- [13] Turner PA, Tomé CN. *Acta Mater* 1994;42(12):4143–53.
- [14] Rietveld HM. *J Appl Crystallogr* 1969;2:65–71.
- [15] Kröner E. *Z Phys* 1958;151(4):504–18.
- [16] Reuss A. *Z Angew Math Mech* 1929;9:49–58.
- [17] Bollenrath F, Hauk V, Müller EH. *Z Metallkd* 1967;58:76–82.